Journal of Medicinal Chemistry

pubs.acs.org/jmc Article

Development of Orally Efficacious Allosteric Inhibitors of TNFα via Fragment-Based Drug Design

Justin D. Dietrich,* Kenton L. Longenecker, Noel S. Wilson, Christian Goess, Sanjay C. Panchal, Steven L. Swann, Andrew M. Petros, Adrian D. Hobson, David Ihle, Danying Song, Paul Richardson, Kenneth M. Comess, Philip B. Cox, Amanda Dombrowski, Kathy Sarris, Diana L. Donnelly-Roberts, David B. Duignan, Arthur Gomtsyan, Paul Jung, A. Chris Krueger, Suzanne Mathieu, Andrea McClure, Vincent S. Stoll, Jill Wetter, John A. Mankovich, Philip J. Hajduk, Anil Vasudevan, Robert H. Stoffel, and Chaohong Sun*

Cite This: *J. Med. Chem.* 2021, 64, 417−429 Read Online

ACCESS | Metrics & More | Article Recommendations | Supporting Information

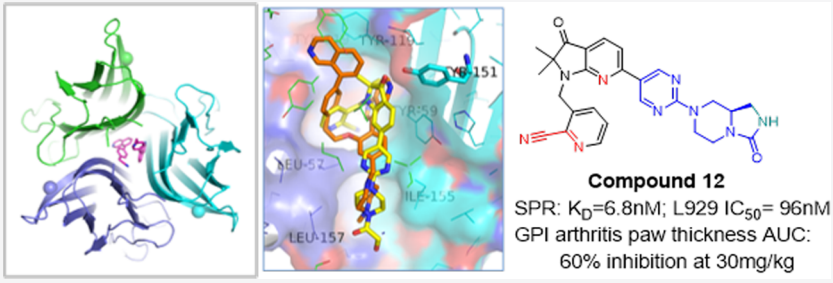

ABSTRACT: Tumor necrosis factor α (TNFα) is a soluble cytokine that is directly involved in systemic inflammation through the regulation of the intracellular NF-κB and MAPK signaling pathways. The development of biologic drugs that inhibit TNFα has led to improved clinical outcomes for patients with rheumatoid arthritis and other chronic autoimmune diseases; however, TNFα has proven to be difficult to drug with small molecules. Herein, we present a two-phase, fragment-based drug discovery (FBDD) effort in which we first identified isoquinoline fragments that disrupt TNFα ligand−receptor binding through an allosteric desymmetrization mechanism as observed in high-resolution crystal structures. The second phase of discovery focused on the *de novo* design and optimization of fragments with improved binding efficiency and drug-like properties. The 3-indolinone-based lead presented here displays oral, *in vivo* efficacy in a mouse glucose-6-phosphate isomerase (GPI)-induced paw swelling model comparable to that seen with a TNFα antibody.

INTRODUCTION

Tumor necrosis factor α (TNFα) is a soluble, homotrimeric cytokine that exerts a wide spectrum of biological activities through interaction with its cognate membrane receptors TNF-R1 and TNF-R2. TNFα, which was originally identified for its cytotoxic and necrotic effects in mouse cancer models over 40 years ago,[1] is now generally associated with proinflammatory responses including activation of NF-κB as well as the JNK and p38-MAPK pathways.[2] Although systemic toxicity of TNFα limits our ability to directly exploit the antitumor effects of the cytokine, the immunomodulatory role of TNFα and associated signaling pathways continue to be an area of intense research.

Approved anti-TNFα drugs,[3] which include monoclonal antibodies as well as fusion proteins, have become the standard of care for rheumatoid arthritis patients that respond poorly to methotrexate monotherapy. The on-label use of anti-TNFα biologics has expanded into other areas of chronic autoimmune diseases such as Crohn's disease, psoriasis, psoriatic arthritis, ulcerative colitis, inflammatory bowel disease, ankylosing spondylitis, and juvenile rheumatoid arthritis.[4]

Even though there is a vast amount of *in vivo* target validation data on anti-TNFα biologics and a clear clinical benefit to patients, only 60−70% of rheumatoid arthritis patients achieve a long-term clinical response.[5] While monoclonal antibodies and fusion proteins have offered a mechanism to directly target cytokines, including TNFα, that have been difficult to inhibit with small molecules, immunogenicity and the production of antidrug antibodies

Received: July 22, 2020
Published: December 30, 2020

https://dx.doi.org/10.1021/acs.jmedchem.0c01280
J. Med. Chem. 2021, 64, 417−429

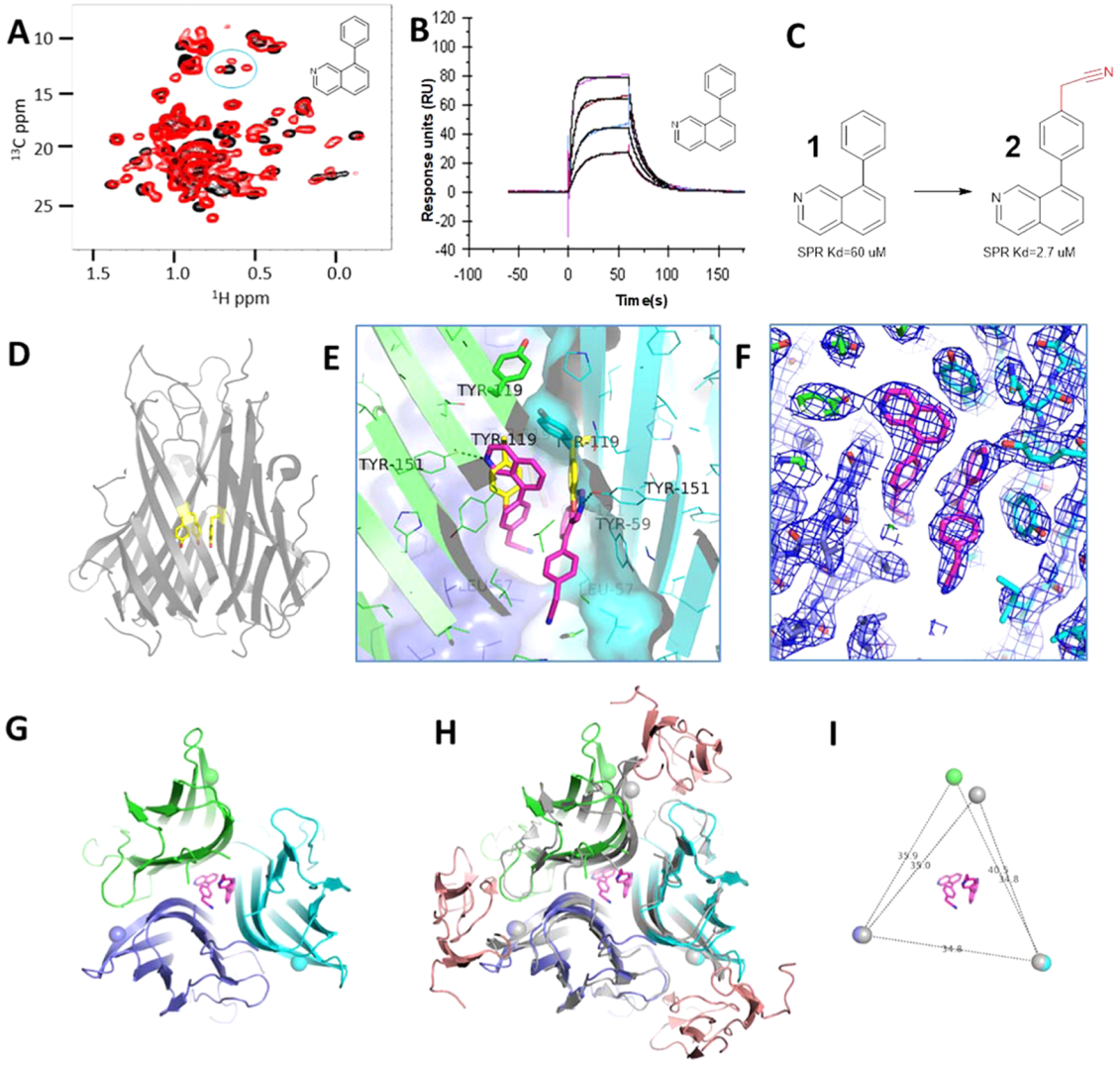

Figure 1. Biophysical and crystallographic characterization of isoquinoline fragments. (A) 2D [^{13}C, ^{1}H]-HSQC spectral overlay of TNFα trimer labeled at the methyl groups of isoleucine (δ only), valine, leucine, and methionine Apo (black) and in the presence of fragment hit compound **1** (red). (B) SPR data of compound **1** binding to TNFα. (C) Structures and binding affinities of initial fragment hit, compound **1**, and compound **2** from the first round of SAR. (D) Side view of apo trimeric TNFα structure with the symmetric Tyr119 (yellow) side chains in the central core. (E) Structure of the compound **2** (magenta) complex with positions of Tyr119 (green for monomer A and cyan for monomer B) from Apo (yellow). (F) Electron density for compound **2** complex (contour 1 sigma). (G) Trimeric view of the compound **2** complex. (H) Overlay of the compound **2** complex with symmetric TNFα:TNF-R1 complex (gray, brown) with positions of Val91 (sphere) for each TNFα monomer. (I) Disrupted trimeric symmetry represented by distance differences for positions of Val91 for compound complex (colors) compared to apo (gray). In each cartoon of the complex with compound **2**, TNFα monomer A is green, monomer B is cyan, and monomer C is dark blue. The PDB code for **2** bound to TNFα trimer is 6 × 81.

are a contributing factor for many adverse events and secondary failures of anti-TNFα biologics.

The first series of small-molecule inhibitors of TNFα, exemplified by SPD-304, was reported by He et al. of Sunesis in 2005.[6] These inhibitors were reported to induce subunit disassembly of trimeric TNFα and subsequent inhibition of the TNFα pathway in biochemical and cell-based assays.[6] Although the compounds displayed only moderate affinity and poor physicochemical properties, this landmark discovery was the first to suggest that TNFα was indeed a druggable target and that binding to this protein could result in decreased binding to its cognate receptor TNF-R1, with a concomitant reduction in proinflammatory responses. Since the disclosure by Sunesis in 2005, there have been multiple reports focused on expanding the number of scaffolds capable of binding directly to TNFα dimer in a similar manner as SPD-304; however, those molecules also suffer from poor overall physicochemical properties that limit their use for *in vivo* proof-of-concept experiments.[7−10] Small molecules that show inhibition of the TNFα pathway have generally been limited to uncharacterized inhibitors of TNFα cell-based assays as well as inhibitors of kinases associated with p38 or MAPK signaling.[6,9,11−14] Despite the incentives associated with small-molecule inhibition of the TNFα pathway, molecules that directly bind and inhibit any form of TNFα were not forthcoming until the report by O'Connell et al. in 2019 describing small molecules that bind to and stabilize an asymmetric population of the trimer.[15] Herein, we present two additional series of molecules that exploit and stabilize this asymmetric form of the protein.

https://dx.doi.org/10.1021/acs.jmedchem.0c01280
J. Med. Chem. 2021, 64, 417−429

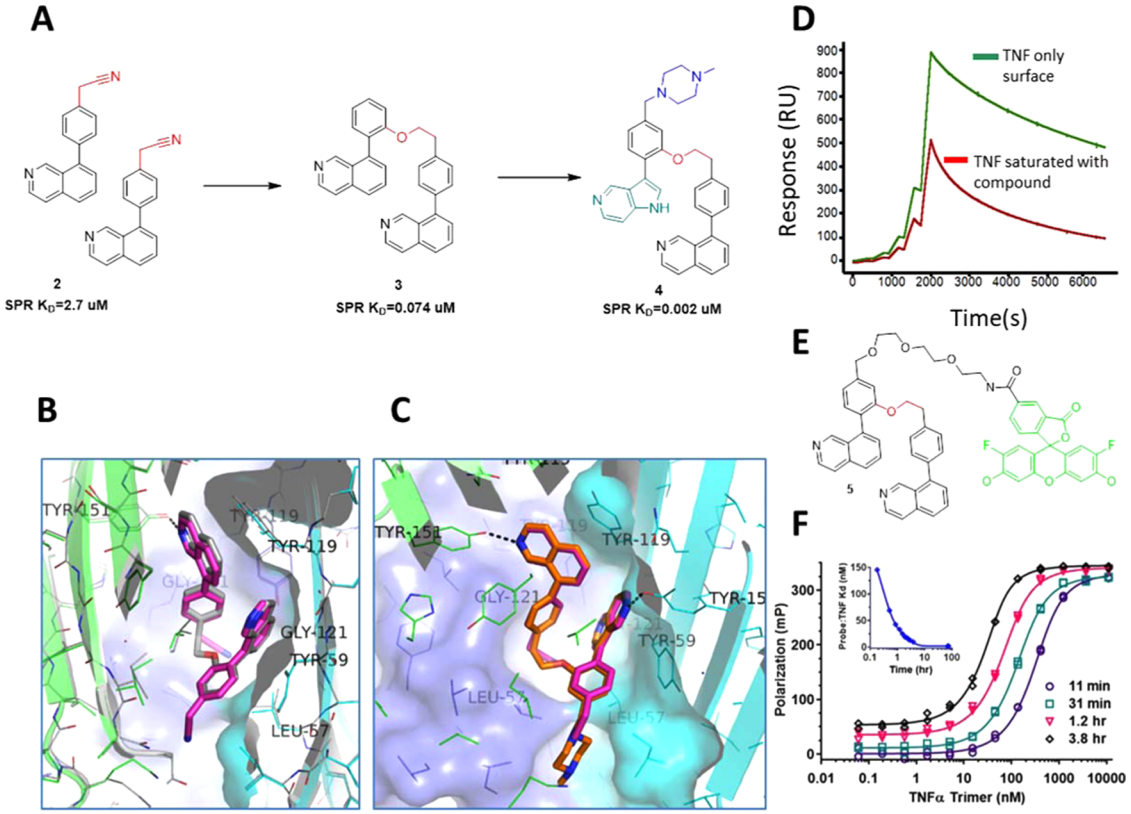

Figure 2. Affinity maturation of isoquinoline fragments. (A) Evolution of isoquinoline compounds from two fragments to linked scaffolds. (B) Binding pose is maintained in the overlay of compound **2** complex (magenta) and crystal structure of linked compound **3** complex (gray). (C) Structural comparison of compound 2 complex (magenta) with the crystal structure of optimized compound **4** (orange). (D) Inhibition of receptor binding by compound **4** as a measure by SPR. (E) Structure of isoquinoline FP probe. (F) FP assay probe displaying the time-dependent increase of binding affinity. The PDB code for compound **4** bound to TNFα trimer is 6 × 82.

RESULTS

Fragment-Based Screening of the Homotrimer of TNFα Ligand. To identify novel chemical matter that binds TNFα, we employed a 2D protein-based NMR fragment screen on an 18,000-member fragment library (MW < 250, MW_{avg} = 204, HBD < 5, HBA < 5, *c*Log*P* < 4, *c*LogP_{avg} = 1.6) against the trimeric form of TNFα. The screen was carried out by adding fragments, initially as mixtures, to TNFα protein, which had been isotopically labeled with ^{13}C at the methyl groups of Ile (δ only), Val, Leu, and Met, with the goal of looking for perturbations in the ^{13}C-HSQC spectrum. Upon deconvolution of the mixtures, we identified 11 fragments (0.06% hit rate) that, upon addition to TNFα, exhibited significant perturbations in the protein spectrum. Compared to other fragment campaigns, a 0.06% hit rate is quite low and can be associated with an overall low ligandability score for TNFα. Subsequently, we obtained binding affinities and kinetic profiles for each compound against TNFα using surface plasmon resonance (SPR). The most promising hit was isoquinoline **1**. Upon addition of compound **1** to TNFα, we observed splitting of certain resonances into three distinct signals (Figure 1A), which suggested that binding of compound **1** may, in fact, disrupt the trimer interface of the TNFα complex. By SPR, compound **1** showed an equilibrium dissociation constant (K_D) of 60 μM for the TNFα trimer (Figure 1B; k_{on} = 1300 1/M·s, k_{off} = 0.0781 1/s). This equated to a surprisingly high binding efficiency index[16] (BEI) of 20.6, a ligand efficiency (LE) of 0.37, and a lipophilic lipid efficiency (LLE) of 0.51. In addition, thermal shift analysis (TSA) of TNFα in complex with compound **1** showed a statistically significant ~2 °C maximum shift.

Without structural information to guide the design, initial optimization focused on substitutions on the phenyl portion of compound **1**. After evaluating approximately 40 analogues, the 4-methylcyano substitution in compound **2** (Figure 1C) improved the affinity roughly 20-fold (SPR K_D = 2.70 μM, k_{on} = 705 1/M·s, k_{off} = 0.0019 1/s) and improved the overall BEI (22.8), LE (0.41), and LLE (2.45). The gain in affinity was attributed to an approximately 40-fold slower off-rate and 2-fold slower on-rate. In TSA, compound **2** showed stabilization of TNFα with an observable ~4 °C shift. The improvement in affinity and solubility of compound **2** were contributing factors in obtaining a high-resolution cocrystal structure of compound **2** bound to TNFα trimer.

Structural Analysis of TNFα Desymmetrization upon Fragment Binding. The crystal structure revealed that two copies of compound **2** were bound and surrounded in a central cavity formed by convergence of the three TNFα monomers (Figure 1D), where one monomer is shifted from its pseudo-symmetric position. In the center of the trimer interface observed in the apo structure of TNFα, tyrosine 119 from all three monomers cluster together with each hydroxyl proton engaging in a hydrogen bond with the backbone carbonyl of glycine 121. In the structure with compound **2** bound, tyrosine 119 from monomer A rotates ~180° and tyrosine 119 from monomer B rotates ~45° resulting in the formation of a large hydrophobic pocket where two copies of the fragment cooperatively bind (Figure 1E–G). The isoquinoline ring of

https://dx.doi.org/10.1021/acs.jmedchem.0c01280
J. Med. Chem. 2021, 64, 417−429

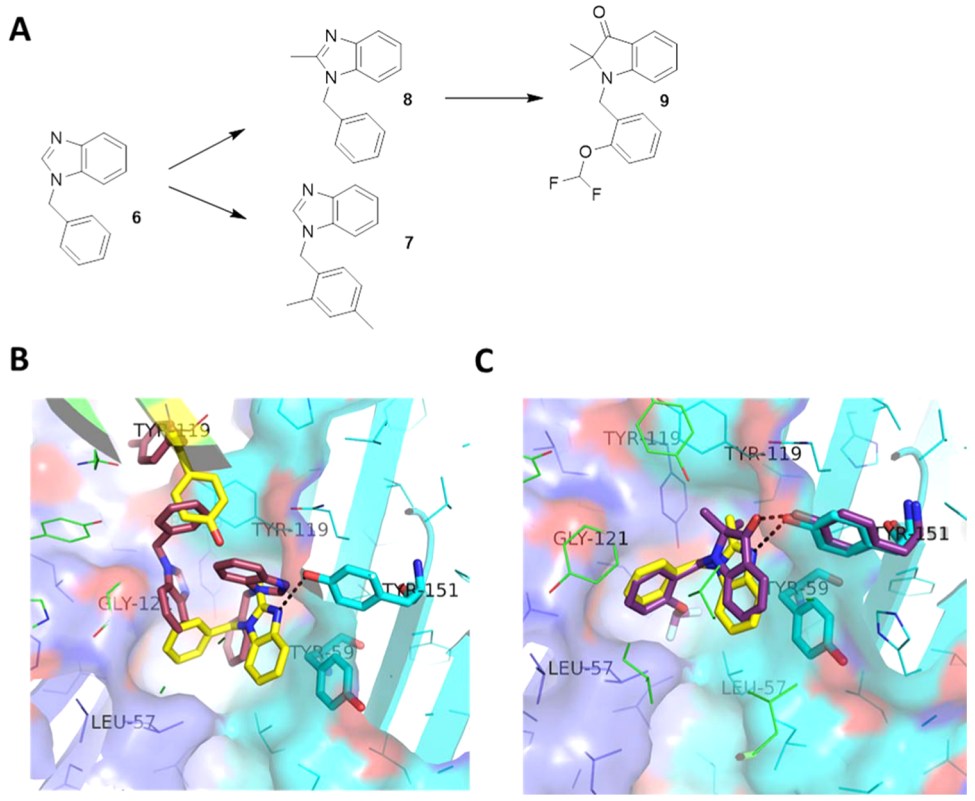

Figure 3. Two binding modes of benzimidazole fragments and indolinone. (A) Compound progression. (B) Crystal structure overlay of compound **6** complex (mauve) as two copies and compound **8** (yellow) as one copy, where the position of Tyr119 for monomer A is highlighted with a compound color for each binding mode. (C) Overlay of benzimidazole compound **8** (yellow) and crystal structure of indolinone compound **9** (purple). The PDB code for **6** bound to TNFα trimer is 6 × 83. The PDB code for **9** bound to TNFα trimer is 6 × 85.

each copy utilizes the hydrophobic void created when the tyrosine residues move and the two fragment copies engage each other through mutual, intermolecular edge-to-face interactions involving both the phenyl and isoquinoline moieties. Each of the isoquinoline copies is anchored into the site by a single hydrogen bond to tyrosine 151 from monomers A and B and two edge-to-face π-interactions between the cyanophenyl of each compound copy with tyrosine 59 of monomers A and B. The 4-methylcyanophenyl ring at the 8-position of copy 1 extends into a hydrophobic cleft formed by leucine 157 and isoleucine 155 from monomer A, isoleucine 155 from monomer B, and leucine 57 and leucine 157 from monomer C and projects the cyano group toward a water channel. The cyanomethyl from copy 2 is in proximity to provide an edge-to-face π-interaction with the isoquinoline from copy 1.

When compared to the previously published structures of apo-TNFα,[17] it is apparent that the binding of compound **2** disrupts the threefold symmetry of the complex (Figure 1H,1I). The interatomic distance between the α carbon of valine 91 between different monomers averages 34.9 angstroms (A−B = 34.8 Å, B−C = 34.8 Å, and C−A = 35.0 Å). By comparison, the structure of TNFα bound to compound **2** is much more asymmetric as the distance between the three valine 91 residues varies from 34.8 to 40.5 Å (A−B = 40.5 Å, B−C = 34.8 Å, and C−A = 35.9.5 Å). This suggests that upon ligand binding, monomer A (Figure 1H, green) is perturbed away from the other monomers of the complex. The asymmetric form of the protein is very similar to that most recently described by O'Connell et al. where they measured interatomic shifts between 5.6 and 9.5 Å for residues in the APO and UCB-6876 bound forms of the protein.[15]

Structure-Based Optimization of Isoquinoline Fragments. In light of this structural information, we explored a focused linking strategy to connect each copy of compound **2** with an appropriate tether that could potentially provide a large boost in potency.[18] A few analogues exploring linker positioning, length, and atom types were evaluated. From this exercise, it was clear that the most efficient position to link was between the ortho-position of the C-ring on copy 1 and the para-position of the C-ring on copy 2. The most potent linked compound from this exercise, compound **3** (Figure 2A), contains a 3-atom ethoxy linker, which resulted in a 36-fold boost in binding affinity (SPR K_D = 0.074 μM, k_{on} = 1020 1/M·s, k_{off} = 0.000075 1/s) and an observed ΔT_m of 7 °C in TSA. We were able to obtain a cocrystal structure with compound **3** that revealed that it retained the binding pose of the individual fragment moieties (Figure 2B); however, efficiency calculations proved to be much less favorable (BEI = 13.3, LE = 0.24, and LLE = −1.7). Knowing that the original fragments bound two copies to the protein and in a cooperative fashion, we hypothesized that it was more appropriate to recalculate both BEI and LE with the total molecular weight or number of atoms bound. The recalculated efficiency metrics for compound **2** are BEI = 11.4 and LE = 0.21. Comparing the affinity and efficiency with the recalculated values still resulted in only a modest improvement; however, having a linked compound provided a scaffold with the potential to optimize each isoquinoline moiety independently of the other. There was also an opportunity to

https://dx.doi.org/10.1021/acs.jmedchem.0c01280
J. Med. Chem. 2021, 64, 417−429

improve affinity and efficiency through SBDD by exploiting the water channel that the cyanomethyl group projected toward in the crystal structure of compound **2** bound to the TNFα trimer. To this end, we looked for cyano replacements that could positively interact with the hydrophobic walls of the channel while also trying to incorporate polarity to decrease the overall lipophilic character of compound **3**. We also aimed to improve our overall drug-like properties by substituting each of the isoquinoline moieties with other bicyclic ring systems. *N*-Methylpiperazine was identified as an optimal replacement for the cyano moiety and found that a 5-azaindole could replace one of the isoquinoline rings to form compound **4**, which displayed a further 50-fold improvement in affinity (K_D = 2 nM, k_{on} = 5710 1/M·s, k_{off} = 0.000012 1/s) and a ΔT_m in TSA of greater than 15 °C. The cocrystal structure of compound **4** bound to the TNFα trimer (Figure 2C) showed that the methylpiperazine ring very efficiently filled the water channel and that the 5-azaindole moiety maintained the hydrogen bond with tyrosine 151 of monomer B. The N−H of the azaindole also provided an additional hydrogen bond donor to engage the hydroxyl of tyrosine 119 from monomer C. The calculated BEI = 15.7, LE = 0.29, and LLE = 2.29 were all improved in comparison to compound **3**. Furthermore, compound **4** displayed an IC_{50} of 128 nM in a cell-based TNFα-induced L929 cytotoxicity rescue assay and an IC_{50} of 89 nM in an NF-κB inhibition assay.[2]

To further interrogate the functional relevance of direct binding of small molecules to TNFα, compound **4** was analyzed by SPR for its ability to inhibit binding of TNF-R1 to TNFα. The binding response of TNF-R1 for TNFα was first measured by flowing TNF-R1 over immobilized TNFα alone and with TNFα complexed with compound **4**. The results show that the maximum binding response of TNF-R1 decreased when immobilized TNFα was complexed with compound **4**, suggesting that these molecules indeed inhibit the binding of TNFα to its cognate receptor (Figure 2D). As the compound is completely engulfed by TNFα, we surmise that the conformational shift of the trimer disposition is responsible for the decrease in receptor binding.

Unfortunately, compound **4** had poor physicochemical properties, high clearance, and poor oral exposure in mice and, therefore, could not be used for *in vivo* efficacy studies. Compound **3**, however, displayed suitable properties to develop fluorescent probe **5** (Figure 2E) that was constructed via a PEG2-ethanolamine linker and amide coupling to an Oregon green fluorophore (see the Supporting Information). Although the isoquinoline series did not provide drug-like properties suitable for *in vivo* target validation or efficacy, the fluorescence polarization assay developed from this probe served as the primary binding assay that supported an expanded medicinal chemistry effort. Consistent with the slow on-rate observed for compound **4** in SPR, the probe compound showed a time-dependent increase in binding affinity (Figure 2F).

Identification of Structurally Related Benzimidazole Fragments with Two Different Binding Modes. With a validated mechanism of allosterically inhibiting TNFα by stabilizing an inactive form of the trimer, the focus of medicinal chemistry efforts shifted toward finding an alternative scaffold with better drug-like properties. To find new starting points, we revisited our original fragment hits. Compound **6**, an *N*-benzylbenzimidazole fragment (Figure 3A), had originally been deprioritized due to its weak affinity (SPR K_D = 300 μM) and lower efficiency (BEI = 16.7, LE = 0.31, LLE = 0.42) compared to isoquinoline **1**. We leveraged parallel chemistry to look at substitutions around the benzyl ring and identified some fragment analogues in our internal repository with a 2-substitution pattern. The SAR around the *N*-benzyl portion was flat, and only a 2,4-dimethylbenzyl substituent, compound **7**, offered any improvement in affinity (SPR K_D = 106 μM); however, the overall efficiency was roughly the same and the lipid efficiency was less favorable (BEI = 16.8, LE = 0.31, and LLE = −0.13). Not surprising at the time, compound **8** (SPR K_D = 325 μM, BEI = 15.7, LE = 0.28, LLE = 0.11), which contained only a 2-methyl substituent on the benzimidazole ring, displayed similar affinity and efficiency when compared directly to compound **6**. Cocrystal structures of each of these three fragments bound to the TNFα trimer show a similar overall shifted disposition of the trimer but two distinct binding modes. The two benzimidazole fragments, **6** and **7**, that did not contain a substituent at the 2-position of the benzimidazole ring bound in a similar fashion as isoquinoline fragment **2** (Figure 3B). Two copies of the fragment bound to the trimer, accepting a hydrogen bond from tyrosine 119 in both monomers A and B and showing distinct cooperative binding via $\pi-\pi$ interactions between the two copies of the fragment. In a similar manner to the isoquinoline series, the two copies of benzimidazole fragments leverage intermolecular interactions with each other to stabilize an asymmetric trimer where monomer A is perturbed away from monomers C and B.

When the 2-methyl was present in compound **8**, however, only one copy of the fragment was bound (Figure 3B). This structure revealed that compound **8** provided a single hydrogen bond acceptor to engage tyrosine 151 from monomer B with the C-ring of the benzimidazole making a face-to-face π-stacking interaction with tyrosine 59 from monomer B. The C3−C4 carbons of the benzyl moiety engaged tyrosine 59 from monomer A with an edge-to-face $\pi-\pi$ interaction. A notable difference was seen in tyrosine 119 in monomer A. Instead of being rotated 180° as seen in the fragments that bound two copies, it appeared in the same conformation as the APO structure; however, it was shifted 5.1 angstroms away from monomer C and in position to stack with tyrosine 119 of monomer B (Figure 3B). When the structures of benzimidazoles **6** and **8** were superimposed, it appeared that the addition of an ortho substituent on the benzyl portion of **8** would provide an even stronger brace and fill the hydrophobic space below the C-ring of the benzimidazole, which is occupied in the structure of benzimidazole **6**. At the time, similar benzyl substitutions at the ortho-position were disclosed by UCB pharma.[15,19,20]

Structural Insights Lead to 3-Indolinone Core. Based on the structural insights gained from the cocrystal structures of compounds **6** and **8** bound to TNFα, we focused on identifying additional fragments that satisfied a pharmacophore model, whereby a biaryl system, like in **6** and **8**, was maintained along with a similar positioning of a H-bond acceptor. We were able to identify a number of scaffolds from this exercise that maintain this central pharmacophore including indolinone **9** and also a closely related indazolone scaffold[21] that shares very similar SAR and will be reported in detail in a separate publication. In this report, the indolinone series is being used as a representative example to map out the critical interactions needed to develop a fragment scaffold into an inhibitor with suitable properties for *in vivo* studies.

https://dx.doi.org/10.1021/acs.jmedchem.0c01280
J. Med. Chem. 2021, 64, 417−429

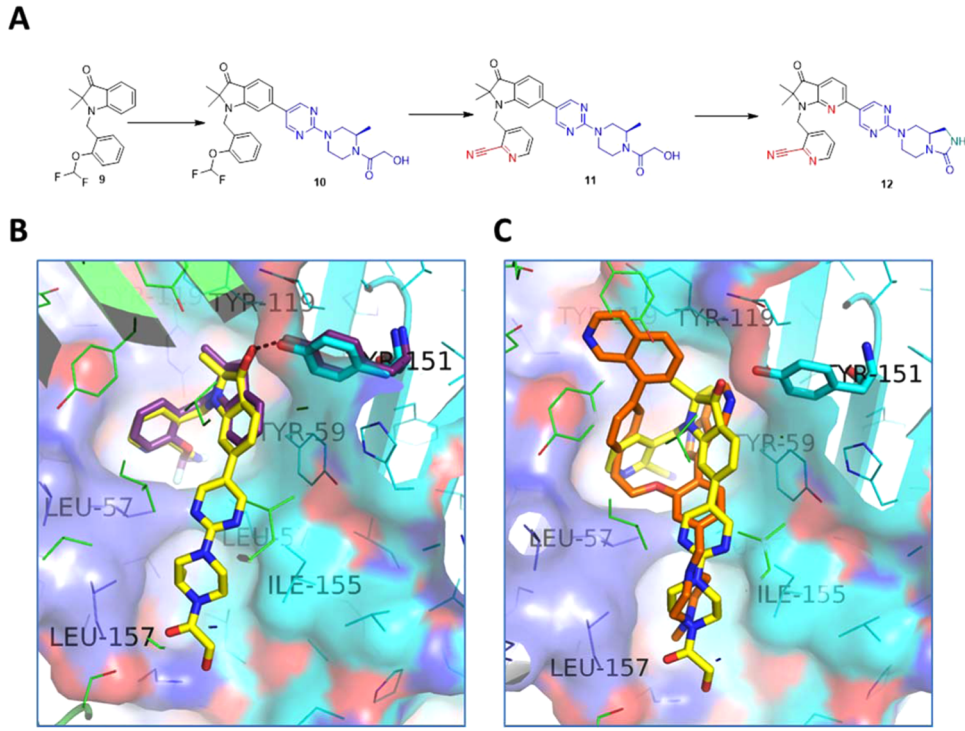

Figure 4. Optimization of indolinone fragment. (A) Elaboration of highlighted compounds. (B) Structural overlay of compound **9** (purple) and crystal structure of compound **11** (yellow). (C) Comparison of binding pose in crystal structures for indolinone compound **11** (yellow) and isoquinoline compound **4** (orange). The PDB code for **11** bound to TNFα trimer is 6 × 86.

The indolinone series was developed from indolinone **9** that binds the TNFα trimer with an SPR K_D = 19 μM (k_{on} = 697 1/M·s, k_{off} = 0.013 1/s, BEI = 14.9, LE = 28.7, LLE = −0.21). As expected, in the solved cocrystal structure with TNFα trimer, indolinone **9** binds in a similar fashion to benzimidazole **8** where the carbonyl oxygen interacts with tyrosine 151 through a single hydrogen bond (2.6 Å) and the C-ring of the indolinone π-stacks with tyrosine 59 (Figure 3C). The ortho-difluoromethoxy group occupies the space under C7 of the indolinone ring. Tyrosine 119 from monomer A is in a similar position to that observed in the cocrystal structure of benzimidazole **8**. Although the overall efficiency was lower than benzimidazole **8**, indolinone **9** exhibited kinetics in the SPR experiment and yielded an IC_{50} of 5.3 μM in the FP binding assay developed from probe **5**. In addition, the sp^3 carbon of the indolinone offered an alternative trajectory to potentially engage tyrosine 119 of monomer A. The overall properties of indolinone **9** are not in line with ideal fragment properties found in our stringently designed fragment libraries;[22] however, once we understood that the binding site in the center of the trimer was highly hydrophobic in nature with a relatively large volume, and an adjacent water channel could be exploited to balance out the physicochemical properties as fragments were grown, we allowed the properties of our *de novo* fragments to expand outside of the Ro3 chemical space.

Structure-Based Optimization of Indolinone 9 and Pharmacokinetic Analysis. Structure-based optimization of indolinone **9** commenced with building into the same water channel that was exploited in isoquinoline **4**. A 5-pyrimidine linked to the 6-position of the 3-indolinone was found to be optimal and provided a trajectory to investigate multiple amine substitutions at the 2-position. We focused on piperazine- and morpholine-like secondary amines based on our knowledge of the SAR in the isoquinoline series and identified compound **10** that utilized a pyrimidine linker and placed an (*R*)-2-hydroxy-1-(2-methylpiperazin-1-yl)ethanone into the water channel (Figure 4B). Compound **10** displayed an IC_{50} = 189 nM in the FP binding assay and 146 nM potency in the L929 assay. Analysis of the binding kinetics by SPR (K_D = 1.3 nM, BEI = 15.8, LE = 0.31, LLE = 3.9) showed that compound **10** was driven by a particularly long half-life (k_{off} = 0.0000045 1/s, $t_{1/2}$ = 42.8 h) and balanced an ∼2-fold slower on-rate (k_{on} = 3380 1/M·s) in comparison to isoquinoline **4** (k_{on} = 5710 1/M·s). Compound **10** was dosed IV and orally to mice at 1 mg/kg and found to have low total blood clearance, good oral bioavailability (F(%) = 75.4%), and an oral half-life of 4.7 h (Table 1). However, compound **10** was associated with high *in vitro* intrinsic clearance in mouse and human microsomes ($CL_{int,u}$ = 101 and 137 L/h/kg), high unbound clearance, low solubility in phosphate buffer (1.2 μM), low fraction unbound (fu) in plasma (0.00293), and a low oral unbound AUC of 6.86 ng·h/mL.

The next stage of optimization focused on maintaining affinity for the target while improving physicochemical properties. Substitution of the ortho-trifluoromethoxy ring with a picolinonitrile provided compound **11** that performed marginally better in the binding and cell-based assays (FP assay IC_{50} = 163 nM, L929 assay IC_{50} = 113 nM). The SPR K_D of compound **11** (K_D = 7.3 nM, BEI = 15.9, LE = 0.30, and LLE = 5.2) showed a loss of approximately 6-fold in affinity that was attributed to an on-rate (k_{on} = 442 1/M·s) that was an order of magnitude slower than that observed for compound **10** and was balanced by a marginally slower off-rate (k_{off} = 0.0000031 1/s, $t_{1/2}$ = 62.3 h). Reduction in the overall lipophilicity resulted in an improvement in lipid efficiency (LLE = 5.2) and solubility (48.4 μM in phosphate buffer at pH = 7.4) and higher fu in plasma (0.137). Pharmacokinetic experiments in

https://dx.doi.org/10.1021/acs.jmedchem.0c01280
J. Med. Chem. 2021, 64, 417−429

Table 1. SPR Kinetic Data, FP Data, and L929 Data

	Structure	SPR K_D (nM)	k_{on} ($M^{-1}s^{-1}$)	k_{off} (s^{-1})	BEI	LE	LLE	FP IC_{50} (nM)	L929 IC_{50} (nM)
1		60,000	1300	$7.8x10^{-2}$	20.6 10.3	0.37 0.185	0.5	25,300	
2	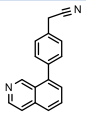	2,700	705	$1.9\ x10^{-3}$	22.8 11.4	0.41 0.205	2.5	7,960	
3	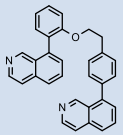	74	1,020	$7.5\ x10^{-5}$	13.3	0.24	-1.7	1,350	
4	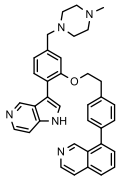	2.4	5,710	$1.2\ x10^{-5}$	15.7	0.29	2.3	29	128
6		300,000	NA	NA	16.7 8.35	0.31 0.155	0.4	204,000	
7		106,000	NA	NA	16.8 8.4	0.31 0.155	-0.1		
8		325,000	NA	NA	15.7	0.28	0.1		
9	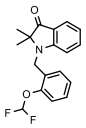	19,000	697	$1.3\ x10^{-2}$	14.9	0.29	-0.2	5,300	NA
10	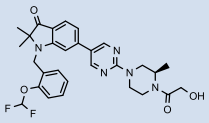	1.3	3,380	$4.5\ x10^{-6}$	15.8	0.31	3.9	189	146
11	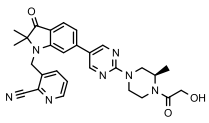	7.3	442	$3.1\ x10^{-6}$	15.9	0.30	5.2	163	119
12	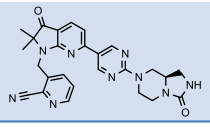	6.8	82,800	$5.6\ x10^{-4}$	16.5	0.31	6.8	71	99

mouse yielded an oral bioavailability of 50.8% for compound **11**, but clearance was high, which contributed to a low oral unbound AUC similar to compound **10**. The cocrystal structure of compound **11** complexed to TNFα trimer shows that the picolinonitrile moiety occupies the same hydrophobic space as the ortho-difluoromethoxy phenyl (Figure 4C) and that the (*R*)-2-hydroxy-1-(2-methylpiperazin-1-yl)ethanone group is once again able to reach deeply into the water channel. A further improvement in physicochemical properties, activity, unbound clearance, and unbound oral exposure (42.4 ng·h/mL) was realized when the (*R*)-2-hydroxy-1-(2-methylpiperazin-1-yl)ethanone was replaced with the bicyclic (*R*)-hexahydroimidazo[1,5-α]pyrazin-3(2*H*)-one in compound **12**. This compound showed over 2-fold improvement in the FP binding assay (IC_{50} = 71 nM) and was equipotent to compound **11** in the L929 assay (IC_{50} = 99 nM). The SPR K_D was almost identical (K_D = 6.8 nM, BEI = 16.5, LE = 0.31, and LLE = 6.8) to compound **11**; however, the overall profile was very different (k_{on} = 82800 1/M·s, k_{off} = 0.00056 1/s, $t_{1/2}$ = 0.9 h). As compounds were optimized for drug-like properties and unbound clearance, their SPR profile shifted from slow-on/slow-off kinetics to fast-on/slow-off kinetics that are more typical to that observed in other small-molecule programs. This was unexpected as it was hypothesized that the slow on-rate was protein limiting and was associated with the time required for the protein equilibrium to shift toward the asymmetric

https://dx.doi.org/10.1021/acs.jmedchem.0c01280
J. Med. Chem. 2021, 64, 417−429

Table 2. Mouse Pharmacokinetics (Data Presented as Mean (SD))

	IV (1 mg/kg)					oral (1 mg/kg)					
	$t_{1/2}$ (h)	V_{ss} (L/kg)	AUC (ng·h/mL)	CL_b (L/h/kg)	$CL_{b,u}$[b] (L/h/kg)	$t_{1/2}$ (h)	C_{max} (ng/mL)	T_{max} (h)	AUC (ng·h/mL)	AUC_u (ng·h/mL)	F(%)
10	4.4[a]	2.12 (0.60)	3110 (1570)	0.369 (0.187)	126 (64)	4.7[a]	200 (33)	1.8 (1.8)	2340 (430)	6.86 (1.26)	75.4 (13.8)
11	1.4[a]	17.3 (4.4)	124 (48)	8.77 (3.43)	57.3 (22.4)	2.0[a]	16.7 (7.1)	1.0 (0.0)	62.7 (30.2)	9.60 (4.63)	50.8 (24.5)
12	1.1[a]	2.12 (0.11)	523 (33)	1.92 (0.12)	11.9 (0.8)	1.6[a]	81.7 (23.1)	1.0 (0.0)	263 (15)	42.4 (2.3)	50.4 (2.8)

[a]Half-life reported as the harmonic mean. [b]$CL_{b,u}$ was calculated as CL_b/fu_{blood}, and AUC_u was calculated as AUC × fu_{blood}. For compound **12**, fu,blood = fu,plasma/(blood/plasma ratio). For compounds **10** and **11**, blood/plasma ratio was assumed to be 1.

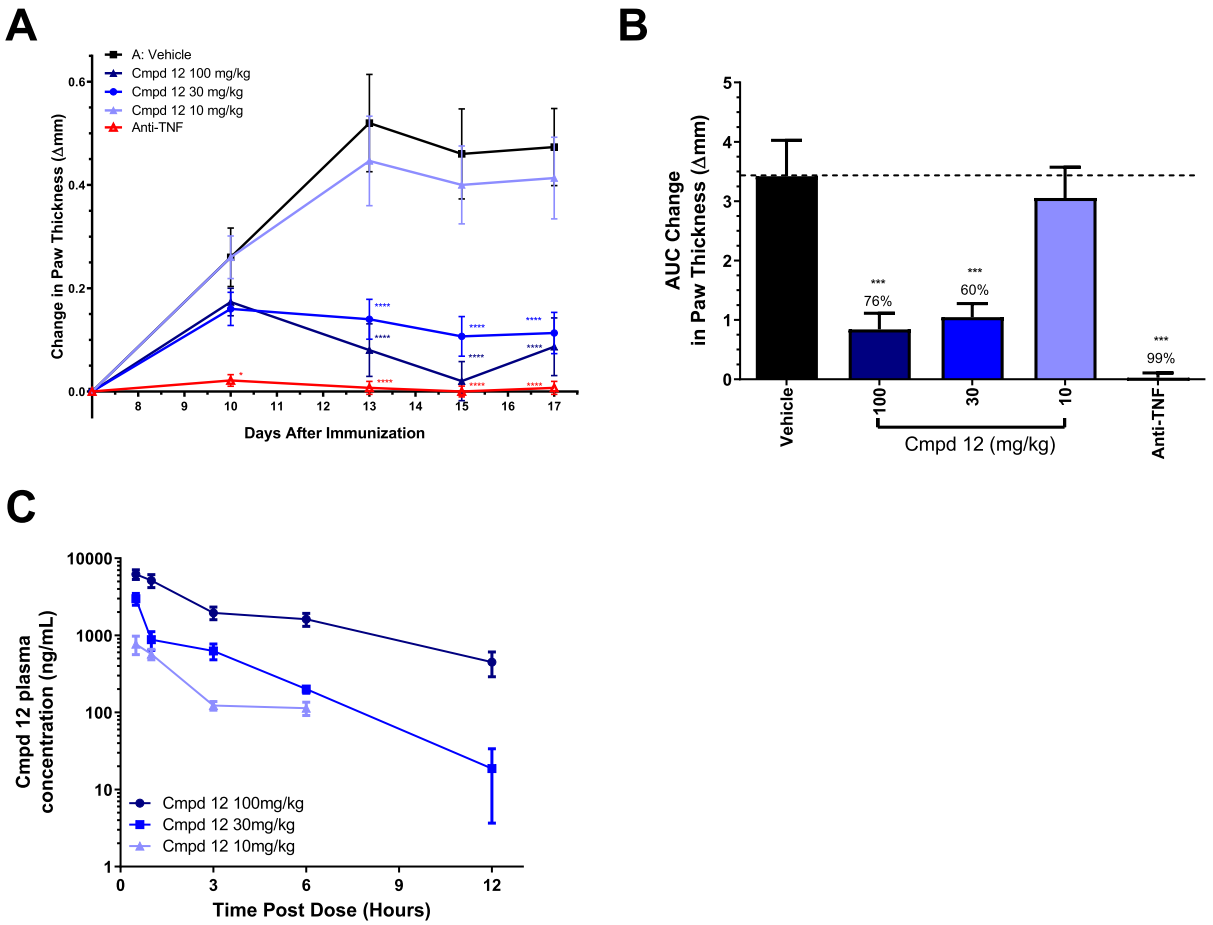

Figure 5. Small-molecule TNF inhibitor compound **12** inhibited paw swelling in the GPI arthritis model. DBA/J mice (n = 15) were immunized with GPI on day 0 and paw swelling assessed. Mice were dosed with compound **12** or anti-TNF antibody 1 h prior to GPI immunization. (A) Change in paw thickness over time with baseline measurement assessed on day 7. Statistical significance evaluated by two-way ANOVA (*p < 0.05, ****p < 0.0001). (B) Area under the curve (AUC) for change in paw thickness from day 7 to 17. Statistical significance evaluated by one-way ANOVA (***p < 0.001). (C) Compound **12** plasma concentration after the final dose on day 17 after GPI immunization.

form. In comparison to compound **11**, the unbound clearance and unbound oral exposure were improved 4.8-fold and 4.4-fold, respectively, for compound **12** (Table 1). Lipid efficiency was improved to 6.8 (Table 2).

Compound 12 *In Vivo* Efficacy in a Mouse Arthritis Model. The *in vivo* efficacy of compound **12** was evaluated in a glucose-6-phosphate isomerase (GPI)-induced mouse arthritis model[23] and compared to anti-TNF antibody treatment. Mice were immunized with GPI resulting in a synchronized onset of disease beginning 10 days after immunization. Mice were dosed with either anti-TNF antibody by intraperitoneal (IP) injection or increasing doses of compound **12** dosed by oral administration. Compound **12** treatment at doses of 30 and 100 mg/kg significantly inhibited paw swelling on days 13, 15, and 17 after GPI immunization (Figure 5A). AUC was calculated from the paw swelling graphs, and both the 100 and 30 mg/kg doses of compound **12** significantly inhibited the paw swelling (Figure 5B). Although anti-TNF antibody appeared to provide a greater inhibition compared to compound **12**, there were no statistically significant differences between the efficacy for either the 30 or 100 mg/kg doses compared to those of anti-TNF treatment. Plasma concentrations of compound **12** were assessed at multiple time points after the final dose on day 17 (Figure 5C). Plasma concentration at C_{max} increased in a dose-dependent manner (10 mg/kg = 767 ng/mL, 30 mg/kg = 2980 ng/mL, 100 mg/kg = 6190 ng/mL) as did AUC_{0-12} (10 mg/kg = 3830 ng·h/mL, 30 mg/kg = 10 200 ng·h/mL, 100 mg/kg = 46 300 ng·h/mL). At 10, 30, and 100 mg/kg, C_{max}, unbound/EC50 = 2.1, 8.3, and 17, respectively.

https://dx.doi.org/10.1021/acs.jmedchem.0c01280
J. Med. Chem. 2021, 64, 417−429

DISCUSSION AND CONCLUSIONS

Inhibition of TNFα and other cytokine signaling pathways such as IL-17, IL-23, and IL-6 have been clinically validated via macromolecular biologic drugs; however, efforts to modulate these pathways with small molecules by directly inhibiting interaction with their cognate receptors have been impeded by the challenges associated with the requirements of a small molecule to disrupt high-affinity, protein−protein interactions. That being said, our experience with TNFα, as well as other reports that describe the identification of ligands that bind cytokines such as IL-17,[24,25] CD40L,[26,27] IL-6,[28] and IL-36,[29] suggests that cytokines may be emerging as a viable target class for small-molecule inhibition. Although robust biochemical tools to study protein−protein interactions may not be as readily available in comparison to more traditional target classes such as enzymes, ion channels, and GPCRs, biophysical methods and affinity-based screening methods have proven capable of identifying viable starting points to initiate medicinal chemistry campaigns. In contrast, identifying starting points for cytokine targets via traditional HTS methods has been elusive, at least in our experience, as many of these targets lack a known binder that is suitable for generating a robust binding assay. In addition, cell-based screens often suffer from ambiguous results arising from off-target activities. We have learned from multiple programs, including this one, aimed at developing small-molecule inhibitors of protein−protein interactions, that biophysical methods, when used to drive a fragment-based approach, offer the greatest chance for success. These biophysical tools include NMR, SPR, ITC, and TSA, all of which can be used to identify small, but efficient, low-affinity (or high-affinity) binders. The low-throughput nature of these methods is somewhat of a disadvantage; however, the robustness of these methods compared to the purely biochemical or cell-based methods more than compensates for this low throughput. As this work illustrates, the combination of 2D NMR and SPR can provide a very detailed view of binding, as it yields not only simple equilibrium binding constants but also kinetic data that can be key for compound optimization. These methods, when combined with X-ray crystallography studies and a robust biochemical assay, exemplify a nearly ideal model for rational drug discovery.

Although our initial effort to optimize isoquinoline fragments did not provide chemical matter with suitable properties for *in vivo* proof-of-concept, the discovery effort generated structural information that was critical in the identification of a desymmetrization mode of action. The isoquinolines also enabled the generation of a robust biochemical- and cell-based screening funnel that was leveraged to discover and advance multiple series with improved drug-like properties. A similar desymmetrization of a trimer as a mode of action has been reported in the identification of binders of another TNF family member, CD40L; however, binding interactions identified in CD40L are quite different from those in TNFα shown here.[26] Our TNF compounds were determined to be selective against other TNF family members including CD40L, TNFβ, and TWEAK (no binding observed in TSA at 50 μM) and also display high levels of selectivity in bioprofiling studies.

Ultimately, our efforts led to the development of a small-molecule TNFα inhibitor, compound **12**, that displays *in vivo* efficacy comparable to a TNFα antibody in a mouse arthritis model. Compound **12** utilizes a mechanism in which binding to the TNFα interface induces desymmetrization of the trimer and results in allosteric modulation of the trimer interaction with its cognate receptor. Although anti-TNFα biologics continue to make a remarkable impact on patients who have chronic autoimmune diseases, the majority of patients do not realize long-term remission of disease because of immunogenicity and the production of antidrug antibodies. A small-molecule inhibitor has the potential to improve long-term remission of disease, and *in vivo* small-molecule tool compounds also have the potential to enable studies aimed at understanding the effects of TNFα inhibition in compartments, such as the brain, where biologic drugs have difficulties penetrating.

EXPERIMENTAL SECTION

Protein Expression and Purification. pT4TNFSt8 plasmid-containing TNFα (residues 77−233) was transformed into *E. coli* BL21(DE3) cell strain. The bacterial fermentation was performed in TB media 50 mg/L of tetracycline at 30 °C for 54 h. For isotopic-labeled protein, the bacterial cells from a fresh transformation plate were grown in M9 media supplemented with 1% ^{13}C-labeled complete media (Silantes, GmbH) and following ^{13}C-labeled amino acid precursors from Cambridge Isotope Laboratories, Inc.: 50 mg/L L-methionine (methyl-^{13}C), 50 mg/L α-ketobutyric acid (methyl-^{13}C), and 100 mg/L α-ketoisovaleric acid (dimethyl-$^{13}C_2$) at 25 °C for 60 h before harvesting.

Protein was purified through Q-Sepharose column with a linear gradient of 25−400 mM NaCl in 50 mM Tris pH 8.0 buffer, followed by Superdex-75 gel filtration column (GE-Healthcare) in 20 mM Tris−HCl, pH 7.8, 25 mM NaCl.

Thermal Shift Assay (TSA) for Compound Characterization. TSA measurements were run on a Light Cycler 480 II instrument from Roche Applied Science. Reactions consisted of 2 μM TNFα in PBS, pH 7.4, a 1/500 dilution of the stock Sypro Orange reagent (S6650, Sigma-Aldrich, supplied as a 5000× concentrate), and 50 μM test compounds, resulting in a final DMSO concentration of 2%. The samples were heated from 20 to 95 °C at a rate of 0.25 °C per second. The T_m values were determined using Roche instrument software in triplicates for each of the tested conditions.

Compound Binding and TNFR-1 Competition via Surface Plasmon Resonance. Compounds were assayed via surface plasmon resonance (SPR) using a Biacore T200 instrument and Biacore 8K (GE-Healthcare and the software provided). Minimal *in vitro* biotinylated human TNFα was immobilized on the neutravidin surface, and multicycle kinetics and single-cycle kinetics modes were used. The compounds were diluted in the running buffer (10 mM Hepes, pH 7.5, 150 mM NaCl, 0.05% Tween-20, and 3% DMSO) and injected in a series of increasing concentrations at a flow rate of 100 μL/min for a contact time of 60 s (for weak compounds) or 200 s (for potent compounds), and dissociation was monitored for up to 500 s (for weak compounds) or 10 000 s (for potent compounds). Sensorgrams were processed and analyzed using Biacore T200 and Biacore 8K evaluation software. The binding curves were fit to determine the equilibrium dissociation constant (K_D) and kinetic constants (k_{on} and k_{off}).

To interrogate the effect of compound to TNFα and TNFR-1 (receptor) interaction, TNFα was immobilized on two separate flow cells as mentioned above. After baseline stabilization, compound **4** was injected at a concentration of 20 nM (10-fold of the K_D) to only one of the flow cells till there was no change in response, suggesting that the immobilized TNFα was completely saturated with compound **4**. Thereafter, TNFR-1 (20 nM highest concentration) was injected over TNFα only and compound 4-saturated TNFα surface to evaluate TNFR-1 binding to apo-TNFα and compound-saturated TNFα.

NMR-Based Fragment Screening. The [^{13}C, ^{1}H]-HSQC spectra used for fragment screening were collected on TNF-α, which was labeled with ^{13}C at the methyl groups of isoleucine (δ only), valine, leucine, and methionine. Spectra for screening were typically collected at 30 °C on protein samples, which were 75 μM

https://dx.doi.org/10.1021/acs.jmedchem.0c01280
J. Med. Chem. 2021, 64, 417−429

monomer concentration (25 μM trimer) in 20 mM Tris, pH 7.5, 50 mM NaCl. All spectra were recorded on Bruker DRX or Avance spectrometers operating at 500 or 600 MHz with cryoprobes. A total of ~18 000 fragments were tested for binding to the TNF-α trimer, initially in mixtures of 30, with each fragment at a concentration of 400 μM in the NMR tube. Those mixtures that elicited significant chemical shift perturbation for the methyl resonances were then deconvoluted to uncover the individual binders.

TNFα Fluorescence Polarization (FP) Binding Assay. The binding of probe compound **5** to TNFα was assayed by monitoring the fluorescence polarization of the probe over a range of concentrations of human TNFα protein. Protein dilutions were made against 1 nM probe compound **5** in a buffer of 47 mM HEPES (pH = 6.5), 47 mM NaCl, 0.9 mM EDTA, 0.007% Triton X-100, and 1% DMSO, and measurements were taken periodically starting after 10 min after mixing the protein with probe and continuing for 75 h. The fluorescence data was fit to a standard binding model using a nonlinear least-squares algorithm.

To assay compounds, a fluorescence polarization (FP)-based competitive binding assay was used with a 20 nM human TNFα trimer and a 1 nM probe compound **5**. Compound plates were prepared by an ECHO liquid dispenser from a 5 mM dimethyl sulfoxide (DMSO) stock. A 1:2 serial dilution of compound concentrations was dispensed in 384-black-well plates from Costar (Corning, NY) with a starting concentration of 100 μM. Assay mixtures (with probe and protein) were incubated in a humidified 37 °C incubator for 18 h and then read on an Envision plate reader with a 337 nM excitation 665/620 nM emission (Perkin Elmer, Waltham, MA). Concentration−response data were analyzed using GraphPad Prism (San Diego, CA).

X-ray Crystallography. Human TNFα (residues 77−233) was concentrated to 15−30 mg/mL in buffer (20 mM Tris, pH 8.0, 100 mM NaCl) and incubated with 2 mM compound overnight. Complexes were screened with commercial reagent kits for cocrystallization conditions using vapor diffusion setups at 293 K. Crystals were harvested from wells with reservoir solution containing 10−20% w/v PEG8000, 0.2 M magnesium acetate, 0.05 M sodium cacodylate, pH 6.5, and rapidly preserved by plunging into liquid nitrogen. X-ray diffraction data were collected at the APS IMCA 17-ID beamline. Structures were solved by molecular replacement using Phaser[30] with data processed and refined using autoPROC[31] and BUSTER[32] software from Global Phasing Ltd. with graphical refinement using COOT.[33] Figures were generated using PyMol (Schrodinger, LLC).

L929 TNFα Cell-Based Assay. L929 cells were plated on the first day into 384-well white plates (Griener #781073; Corning, NY) in the media listed in tissue culture (Supplemental) except with the substitution of 2% FBS (final concentration) and the addition of 4 μg/mL actinomysin D (Sigma-Aldrich) at a concentration of 5000 cells/25 μL/well. Plated cells were incubated for 1 h at 37 °C. Concurrently, 1:2 serially diluted compounds (highest concentration of 50 μM) were pretreated with 60 pg/mL mouse TNFα protein (muTNFα, made in-house) in the 2% FBS media and incubated for 1 h at 37 °C, and then added to the L929 cell plate for incubation overnight at 37 °C. The final concentration of 30 pg/mL muTNFα was used in the assay. The following morning, the cell-compound plates were equilibrated to room temperature and 25 μL/well of CellTiter-Glo 2.0 (Promega, Madison WI) was added to the cell-compound plates. After shaken on an orbital shaker and 15 min incubation in the dark at room temperature, the plates were read on an Envision plate reader set to 0.5 s of luminescence integration time (Perkin Elmer, Waltham, MA). Raw data was normalized to a maximum signal of 30 pg/mL muTNFα with basal levels subtracted out (no treatment with muTNFα). Concentration−response data were analyzed using GraphPad Prism (San Diego, CA). IC_{50} values were derived from a single curve fit to the mean data generated.

Pharmacokinetic Studies in Mice. Male CD-1 mice, weighing 20−25 g (est. 31−44 days old), were obtained from Charles Rivers Laboratories and were socially housed and allowed free access to food and water. Pharmacokinetic studies were conducted in groups of mice; each group contained two animals. These studies were conducted as a singleton study (compound **11**) or a study with cassette dosing of one (compound **10**) or two (compound **12**) additional compounds to the same animal at 1 mg/kg. All groups were dosed with solution formulations including dimethyl sulfoxide, poly(ethylene glycol) 400, polysorbate 80, and 5% dextrose in water. Groups of two mice received either an intravenous dose, administered under isoflurane anesthetic, or an oral dose, administered by gavage. Sequential blood samples were obtained from a tail vein of each animal for 24 h after dosing. Blood was collected and stored frozen until analysis. Compounds were selectively removed from blood using protein precipitation followed by reverse-phase HPLC with MS/MS detection for quantification. Pharmacokinetic parameters after oral dosing were calculated by noncompartmental methods, while pharmacokinetic parameters after IV dosing were calculated by compartmental methods using WinNonlin (version 5.2, Certara USA Inc., St. Louis, MO). All animal studies were approved by the AbbVie Institutional Animal Care and Use Committee (IACUC) and conducted in an AAALAC accredited facility to ensure high standards of animal care and use.

***In Vivo* Arthritis Model.** Male DBA/J mice (Jackson Labs, Bar Harbor, ME) were immunized intradermally at the base of the tail with 100 μL of 1:1 (v/v) emulsion containing 300 μg of glucose-6-phosphate isomerase (GPI) and 200 μg of heat-inactivated *Mycobacterium tuberculosis* H37Ra (Complete Freund's Adjuvant, Difco, Laurence, KS). Mice were dosed orally BID beginning 1 h prior to GPI immunization with compound **12** in 0.5% HPMC/0.02% Tween-80 at the indicated doses. Paw swelling in rear paws was measured using Dyer spring calipers with baseline paw thickness assessed on day 7 after immunization, and additional measurements were assessed on days 10, 13, 15, and 17. On day 17, the mice were bled by tail nick and/or cardiac puncture at 0.5, 1, 3, 6, and 12 h post final dose, and plasma was collected for quantification of compound by HPLC-MS/MS. In addition, mice were dosed with 12 mg/kg anti-TNF antibody by intraperitoneal (IP) injection twice per week beginning 1 h prior to GPI immunization.

Chemistry. All commercially available chemicals and solvents were used without further purification. In general, reaction mixtures were magnetically stirred at the respective temperature under a nitrogen atmosphere. Organic solutions were concentrated under reduced pressure using a Büchi rotovap. Reactions under microwave irradiation conditions were carried out in a Biotage Initiator EXP instrument. Normal phase chromatography was performed on an ISCO CombiFlash Companion MPLC system using RediSep prepacked columns with silica, and reverse-phase chromatography was performed using Chromabond C18 cartridges. Reactions were monitored by thin-layer chromatography using HPTLC Silicagel 60 F254 plates from Merck KGaA and were visualized using 254 nm ultraviolet light and/or exposure to silica gel impregnated with iodine. All new compounds gave satisfactory ^{1}H NMR and LC/MS. On the basis of LC-MS, all final compounds were >95% pure unless otherwise noted. NMR spectra were obtained on a Bruker Avance I 400 MHz, Avance III 500 MHz, or 600 MHz NMR spectrometer using residual signal of deuterated NMR solvent as internal reference; chemical shifts for protons are reported in a parts per million scale downfield from tetramethylsilane. Analytical LC-MS data was obtained using an Agilent 1100 series HPLC system with DAD and SQ mass spectrometer with ESI in positive mode and a scan range of 100−700 amu. Samples were run on a Chromasil 80 ODS-7pH column 4 μm, 40 mm × 2 mm; gradient elution 5−100% B over 10 min; solvent A: H_2O/0.1% TFA; solvent B: acetonitrile/0.1% TFA; flow rate: 0.5 mL/min; temperature: 60 °C. Alternatively, analytical LC-MS was performed on a Thermo MSQ-Plus mass spectrometer and an Agilent 1100/1200 HPLC system with APCI in positive mode and a scan range of 100−1000. The column used was a Phenomenex Kinetex C8, 2.6 μm 100 Å (2.1 mm × 30 mm), at a temperature of 65 °C and a gradient of 5−100% acetonitrile (A) and 0.1% trifluoroacetic acid in water (B) was used, at a flow rate of 1.5 mL/min (0−0.05 min 5% A, 0.05−1.2 min 5−100% A, 1.2−1.4 min 100% A, 1.4−1.5 min 100−5% A. 0.25 min postrun delay). Samples were purified by preparative

https://dx.doi.org/10.1021/acs.jmedchem.0c01280
J. Med. Chem. 2021, 64, 417−429

HPLC on a Phenomenex Luna C8(2) 5 μm 100 Å AXIA column (30 mm × 75 mm) with a gradient of acetonitrile (A) and 0.1% trifluoroacetic acid in water (B), at a flow rate of 50 mL/min (0−1.0 min 5% A, 1.0−8.5 min linear gradient 5−100% A, 8.5−11.5 min 100% A, 11.5−12.0 min linear gradient 95−5% A). Chemical names were generated using ChemDraw Professional 15.0 (Perkin Elmer Informatics).

Compounds **6** and **8** were purchased from commercial sources and are included in our fragment screening collection.

Preparation of 3-((6-Bromo-2,2-dimethyl-3-oxo-2,3-dihydro-1H-pyrrolo[2,3-*b*]pyridin-1-yl)methyl)picolinonitrile (12a). To a solution of 6-bromo-2,2-dimethyl-1*H*-pyrrolo[2,3-*b*]-pyridin-3(2*H*)-one (10 g, 41.5 mmol, preparation #2) in anhydrous DMF (100 mL) at 0 °C was added NaH (2 g, 50.0 mmol). The mixture was stirred for about 20 min at 0 °C. 3-(Bromomethyl)-picolinonitrile (8.99 g, 45.6 mmol) in 10 mL of anhydrous DMF was added. The reaction was heated to 50 °C for 30 min. The reaction was cooled to rt and quenched with 300 mL of ice/water. The mixture was sonicated for 30 min. The solids were filtered off, and the filter cake was washed with excess water. The solid was dried under reduced pressure to afford the title compound (14.34 g, 97% yield); ^{1}H NMR (400 MHz, DMSO-d_6) δ 8.68 (dd, J = 4.6, 1.5 Hz, 1H), 8.00−7.91 (m, 1 H), 7.84 (d, J = 7.8 Hz, 1H), 7.69 (dd, J = 8.1, 4.7 Hz, 1H), 7.02 (d, J = 7.8 Hz, 1H), 4.97 (s, 2H), 1.27 (s, 6H). LC/MS (Table 1; Method **e**) R_t = 0.87 min; MS m/z 357.1 w/Br pattern $[M + H]^+$.

Preparation of (*R*)-3-((2,2-Dimethyl-3-oxo-6-(2-(3-oxohexahydroimidazo[1,5-*a*]pyrazin-7(1*H*)-yl)pyrimidin-5-yl)-2,3-dihydro-1*H*-pyrrolo[2,3-*b*]pyridin-1-yl)methyl)-picolinonitrile (12). To (*S*)-hexahydroimidazo[1,5-*a*]pyrazin-3(2*H*)-one hydrochloride (2.5 equiv, 3.75 mmol) and 2-chloro-5-(4,4,5,5-tetramethyl-1,3,2-dioxaborolan-2-yl)pyrimidine (2.5 equiv, 3.75 mmol) was added anhydrous ethanol (12.0 mL). To this solution was added TEA (11.05 equiv, 16.58 mmol). The reaction was purged with nitrogen and then heated to 95 °C for 2 h. After the starting materials had been consumed as judged by LC-MS analysis, the mixture was concentrated. To the reaction was added 3-((6-bromo-2,2-dimethyl-3-oxo-2,3-dihydro-1*H*-pyrrolo[2,3-*b*]pyridin-1-yl)methyl)picolinonitrile (1.0 equiv, 1.5 mmol), cesium carbonate (4.5 equiv, 6.75 mmol), and $PdCl_2$(dppf)-CH_2Cl_2 (0.1 equiv, 0.150 mmol). Dioxane (12.0 mL) and 6.0 mL of water (6.0 mL) were added. The reaction was purged with nitrogen and degassed. It was heated to 95 °C for 2 h. After the starting materials had been consumed as judged by LC-MS analysis, the mixture was cooled to rt and then concentrated. The crude material was purified by reverse-phase HPLC Luna 70 mm × 30 mm, 5 μm with 0−100% ACN/H_2O 0.1% TFA (42 mL/min). The purified material was free-based by dissolving in DCM and stirring with MP-carbonate (4.0 equiv, load = 2.64 mmol/g) for 2 h. The mixture was filtered and concentrated to give a yellow oil. The oil was precipitated from DCM/heptanes (1:12) to give a yellow solid (0.566 mmol, 37.7% yield). ^{1}H NMR (400 MHz, DMSO-d_6) δ 8.93 (s, 2H), 8.67 (dd, J = 4.7, 1.5 Hz, 1H), 8.00−7.92 (m, 2H), 7.68 (dd, J = 8.1, 4.6 Hz, 1H), 7.37 (d, J = 8.0 Hz, 1H), 6.53 (s, 1H), 5.03 (s, 2H), 4.83−4.75 (m, 1H), 4.75−4.66 (m, 1H), 3.72−3.59 (m, 2H), 3.41 (t, J = 8.7 Hz, 1H), 3.01 (dd, J = 9.3, 4.5 Hz, 1H), 2.92−2.77 (m, 3H), 1.32 (s, 6H). MS (APCI$^+$) m/z = 496.2 $[M + H]^+$.

■ ASSOCIATED CONTENT

Supporting Information

The Supporting Information is available free of charge at https://pubs.acs.org/doi/10.1021/acs.jmedchem.0c01280.

Refinement statistics for the crystal structures of compounds **2**, **4**, **6**, **9**, and **11** bound to TNFα, materials and methods for tissue culture, materials and methods for the NF-κB HEK293 reporter assay, synthetic procedures for the preparation of compounds **1**−**11** (PDF)

Molecular formula SMILES strings (CSV)

Accession Codes

Atomic coordinates and structure factors for the TNFα have been deposited in the Protein Data Bank under the PDB ID codes 6 × 81, 6 × 82, 6 × 83, 6 × 85, and 6 × 86 for compounds **2**, **4**, **6**, **9**, and **11**, respectively, and will be released upon publication.

■ AUTHOR INFORMATION

Corresponding Authors

Justin D. Dietrich − *Research & Development, AbbVie, North Chicago, Illinois 60064, United States;* orcid.org/0000-0002-0703-1817; Phone: 847 937 6507; Email: justin.dietrich@AbbVie.com

Chaohong Sun − *Research & Development, AbbVie, North Chicago, Illinois 60064, United States*; Phone: 847 935 4730; Email: chaohong.sun@AbbVie.com

Authors

Kenton L. Longenecker − *Research & Development, AbbVie, North Chicago, Illinois 60064, United States*

Noel S. Wilson − *Research & Development, AbbVie, North Chicago, Illinois 60064, United States*

Christian Goess − *AbbVie Bioresearch Center, Worcester, Massachusetts 01605, United States*

Sanjay C. Panchal − *Research & Development, AbbVie, North Chicago, Illinois 60064, United States*

Steven L. Swann − *Research & Development, AbbVie, North Chicago, Illinois 60064, United States*

Andrew M. Petros − *Research & Development, AbbVie, North Chicago, Illinois 60064, United States;* orcid.org/0000-0003-1704-415X

Adrian D. Hobson − *AbbVie Bioresearch Center, Worcester, Massachusetts 01605, United States*

David Ihle − *AbbVie Bioresearch Center, Worcester, Massachusetts 01605, United States*

Danying Song − *Research & Development, AbbVie, North Chicago, Illinois 60064, United States*

Paul Richardson − *Research & Development, AbbVie, North Chicago, Illinois 60064, United States*

Kenneth M. Comess − *Research & Development, AbbVie, North Chicago, Illinois 60064, United States;* orcid.org/0000-0003-4198-9372

Philip B. Cox − *Research & Development, AbbVie, North Chicago, Illinois 60064, United States*

Amanda Dombrowski − *Research & Development, AbbVie, North Chicago, Illinois 60064, United States*

Kathy Sarris − *Research & Development, AbbVie, North Chicago, Illinois 60064, United States*

Diana L. Donnelly-Roberts − *Research & Development, AbbVie, North Chicago, Illinois 60064, United States*

David B. Duignan − *AbbVie Bioresearch Center, Worcester, Massachusetts 01605, United States*

Arthur Gomtsyan − *Research & Development, AbbVie, North Chicago, Illinois 60064, United States*

Paul Jung − *Research & Development, AbbVie, North Chicago, Illinois 60064, United States;* orcid.org/0000-0001-9168-6738

A. Chris Krueger − *Research & Development, AbbVie, North Chicago, Illinois 60064, United States*

Suzanne Mathieu − *AbbVie Bioresearch Center, Worcester, Massachusetts 01605, United States*

https://dx.doi.org/10.1021/acs.jmedchem.0c01280
J. Med. Chem. 2021, 64, 417−429

Andrea McClure − *Research & Development, AbbVie, North Chicago, Illinois 60064, United States*
Vincent S. Stoll − *Research & Development, AbbVie, North Chicago, Illinois 60064, United States*
Jill Wetter − *Research & Development, AbbVie, North Chicago, Illinois 60064, United States*
John A. Mankovich − *AbbVie Bioresearch Center, Worcester, Massachusetts 01605, United States*
Philip J. Hajduk − *Research & Development, AbbVie, North Chicago, Illinois 60064, United States*
Anil Vasudevan − *Research & Development, AbbVie, North Chicago, Illinois 60064, United States;* orcid.org/0000-0002-0004-0497
Robert H. Stoffel − *AbbVie Bioresearch Center, Worcester, Massachusetts 01605, United States*

Complete contact information is available at: https://pubs.acs.org/10.1021/acs.jmedchem.0c01280

Notes

The authors declare no competing financial interest.

■ ACKNOWLEDGMENTS

The authors thank Pierre Bodelle of AbbVie for help with protein expression; Rohinton Edalji, former AbbVie employee, for help with protein purification and TSA experiments; Emily Nicholl of AbbVie for help with the TSA assay; Manisha Jhala of AbbVie and Marian T. Namovic of AbbVie for help with the FP assay and L929 cell-based assay; and Mulugeta Mamo, former AbbVie employee, and Ievgeniia Dubrovska of AbbVie for help with crystallization. Use of the IMCA-CAT beamline 17-ID (or 17-BM) at the Advanced Photon Source was supported by the companies of the Industrial Macromolecular Crystallography Association through a contract with the Hauptman-Woodward Medical Research Institute. Use of the Advanced Photon Source was supported by the U.S. Department of Energy, Office of Science, Office of Basic Energy Sciences, under Contract No. DE-AC02-06CH11357. J.D.D., K.L.L., N.S.W., C.G., S.C.P., A.M.P., A.D.H., D.I., D.S., P.L., K.M.C., P.C., A.D., D.L.D.-R., D.B.D., P.J., A.C.K., S.M., A.M., V.S.S., J.W., P.J.H., A.V., K.S., R.H.S., and C.S. are employees of AbbVie. S.S., A.G., and J.A.M. were employees of AbbVie at the time of the study. The design, study conduct, and financial support for this research were provided by AbbVie. AbbVie participated in the interpretation of data, review, and approval of the publication.

■ ABBREVIATIONS

NMR, nuclear magnetic resonance; BEI, binding efficiency index; LE, ligand efficiency; LLE, ligand lipophilic efficiency; FBDD, fragment-based drug discovery; GPI, glucose-6-phosphate isomerase; TNF-R1, tumor necrosis factor receptor 1; TNF-R2, tumor necrosis factor receptor 2; NF-κB, nuclear factor kappa-light-chain-enhancer of activated B cells; JNK, c-Jun N-terminal kinase; p38-MAPK, p38 mitogen-activated protein kinases; HSQC, heteronuclear single quantum coherence; SPR, surface plasmon resonance; TSA, thermal shift analysis; FP, fluorescence polarization; SBDD, structure-based drug design; PEG, poly(ethylene glycol); SAR, structure−activity relationship; AUC, area under the curve; V_{ss}, steady-state volume of distribution; CL, clearance; C_{max}, maximum concentration; F, oral bioavailability; IL-17, interleukin 17; IL-23, interleukin 23; IL-6, interleukin 6; CD40L, cluster of differentiation 40; IL-36, interleukin 36; GPCR, G-protein-coupled receptor; HTS, high-throughput screening; ITC, isothermal calorimetry; TWEAK, TNF-related weak inducer of apoptosis; MPLC, medium-pressure liquid chromatography; LC-MS, liquid chromatography mass spectrometry; DAD, diode array detector; IP, intraperitoneal; DMF, dimethylformamide; DMSO, dimethylsulfoxide; TEA, triethylamine; DCM, dichloromethane

■ REFERENCES

(1) Carswell, E. A.; Old, L. J.; Kassel, R. L.; Green, S.; Fiore, N.; Williamson, B. An endotoxin-induced serum factor that causes necrosis of tumors. *Proc. Natl. Acad. Sci. U.S.A.* **1975**, *72*, 3666−3670.
(2) Hayden, M. S.; Ghosh, S. Regulation of NF-kappaB by TNF family cytokines. *Semin. Immunol.* **2014**, *26*, 253−266.
(3) Lis, K.; Kuzawinska, O.; Balkowiec-Iskra, E. Tumor necrosis factor inhibitors - state of knowledge. *Arch. Med. Sci.* **2014**, *6*, 1175−1185.
(4) Monaco, C.; Nanchahal, J.; Taylor, P.; Feldmann, M. Anti-TNF therapy: past, present and future. *Int. Immunol.* **2015**, *27*, 55−62.
(5) Kalden, J. R.; Schulze-Koops, H. Immunogenicity and loss of response to TNF inhibitors: implications for rheumatoid arthritis treatment. *Nat. Rev. Rheumatol.* **2017**, *13*, 707−718.
(6) He, M. M.; Smith, A. S.; Oslob, J. D.; Flanagan, W. M.; Braisted, A. C.; Whitty, A.; Cancilla, M. T.; Wang, J.; Lugovskoy, A. A.; Yoburn, J. C.; Fung, A. D.; Farrington, G.; Eldredge, J. K.; Day, E. S.; Cruz, L. A.; Cachero, T. G.; Miller, S. K.; Friedman, J. E.; Choong, I. C.; Cunningham, B. C. Small-molecule inhibition of TNF-alpha. *Science* **2005**, *310*, 1022−1025.
(7) Chan, D. S.; Lee, H. M.; Yang, F.; Che, C. M.; Wong, C. C.; Abagyan, R.; Leung, C. H.; Ma, D. L. Structure-based discovery of natural-product-like TNF-alpha inhibitors. *Angew. Chem., Int. Ed.* **2010**, *49*, 2860−28644.
(8) Choi, H.; Lee, Y.; Park, H.; Oh, D. S. Discovery of the inhibitors of tumor necrosis factor alpha with structure-based virtual screening. *Bioorg. Med. Chem. Lett.* **2010**, *20*, 6195−6198.
(9) Alexiou, P.; Papakyriakou, A.; Ntougkos, E.; Papaneophytou, C. P.; Liepouri, F.; Mettou, A.; Katsoulis, I.; Maranti, A.; Tsiliouka, K.; Strongilos, A.; Chaitidou, S.; Douni, E.; Kontopidis, G.; Kollias, G.; Couladouros, E.; Eliopoulos, E. Rationally designed less toxic SPD-304 analogs and preliminary evaluation of their TNF inhibitory effects. *Arch. Pharm.* **2014**, *347*, 798−805.
(10) Keerthy, H. K.; Mohan, C. D.; Sivaraman Siveen, K.; Fuchs, J. E.; Rangappa, S.; Sundaram, M. S.; Li, F.; Girish, K. S.; Sethi, G.; Basappa; Bender, A.; Rangappa, K. S. Novel synthetic biscoumarins target tumor necrosis factor-alpha in hepatocellular carcinoma in vitro and in vivo. *J. Biol. Chem.* **2014**, *289*, 31879−31890.
(11) Richmond, V.; Michelini, F. M.; Bueno, C. A.; Alche, L. E.; Ramirez, J. A. Small molecules as anti-TNF Drugs. *Curr. Med. Chem.* **2015**, *22*, 2920−2942.
(12) Blevitt, J. M.; Hack, M. D.; Herman, K. L.; Jackson, P. F.; Krawczuk, P. J.; Lebsack, A. D.; Liu, A. X.; Mirzadegan, T.; Nelen, M. I.; Patrick, A. N.; Steinbacher, S.; Milla, M. E.; Lumb, K. J. Structural basis of small-molecule aggregate induced inhibition of a protein-protein interaction. *J. Med. Chem.* **2017**, *60*, 3511−3517.
(13) Luzi, S.; Kondo, Y.; Bernard, E.; Stadler, L. K.; Vaysburd, M.; Winter, G.; Holliger, P. Subunit disassembly and inhibition of TNFalpha by a semi-synthetic bicyclic peptide. *Protein Eng., Des. Sel.* **2015**, *28*, 45−52.
(14) Melagraki, G.; Leonis, G.; Ntougkos, E.; Rinotas, V.; Papaneophytou, C.; Mavromoustakos, T.; Kontopidis, G.; Douni, E.; Kollias, G.; Afantitis, A. Current status and future prospects of small-molecule protein-protein interaction (PPI) inhibitors of Tumor Necrosis Factor (TNF) and receptor activator of NF-kappaB Ligand (RANKL). *Curr. Top. Med. Chem.* **2018**, *18*, 661−673.
(15) O'Connell, J.; Porter, J.; Kroeplien, B.; Norman, T.; Rapecki, S.; Davis, R.; McMillan, D.; Arakaki, T.; Burgin, A.; Fox Iii, D.; Ceska, T.; Lecomte, F.; Maloney, A.; Vugler, A.; Carrington, B.; Cossins, B. P.;

Bourne, T.; Lawson, A. Small molecules that inhibit TNF signalling by stabilising an asymmetric form of the trimer. *Nat. Commun.* **2019**, *10*, No. 5795.
(16) Abad-Zapatero, C.; Metz, J. T. Ligand efficiency indices as guideposts for drug discovery. *Drug Discovery Today* **2005**, *10*, 464−469.
(17) Eck, M. J.; Sprang, S. R. The structure of tumor necrosis factor-alpha at 2.6 A resolution. Implications for receptor binding. *J. Biol. Chem.* **1989**, *264*, 17595−17605.
(18) Shuker, S. B.; Hajduk, P. J.; Meadows, R. P.; Fesik, S. W. Discovering high-affinity ligands for proteins: SAR by NMR. *Science* **1996**, *274*, 1531−1534.
(19) Bentley, J. M.; Brookings, D. C.; Brown, J. A.; Cain, T. P.; Gleave, L. J.; Heifetz, A.; Jackson, V. E.; Johnstone, C.; Leigh, D.; Madden, J.; Porter, J. R.; Selby, M. D.; Zhu, Z. Imidazopyrazine derivatives as modulators of TNF activity and their preparation. PCT Int. Appl. WO2014/009296A1, 2014.
(20) Bentley, J. M.; Brookings, D. C.; Brown, J. A.; Cain, T. P.; Chovatia, P. T.; Foley, A. M.; Gallimore, E. O.; Gleave, L. J.; Heifetz, A.; Horsley, H. T.; Hutchings, M. C.; Jackson, V. E.; Johnson, J. A.; Johnstone, C.; Kroeplien, B.; Lecomte, F. C.; Leigh, D.; Lowe, M. A.; Madden, J.; Porter, J. R.; Quincey, J. R.; Reed, L. C.; Reuberson, J. T.; Richardson, A. J.; Richardson, S. E. Imidazopyridine derivatives as modulators of TNF activity and their preparation. PCT Int. Appl. WO2014/009295A1, 2014.
(21) Argiriadi, M.; Breinlinger, E.; Dietrich, J. D.; Friedman, M.; Ihle, D.; Morytko, M.; Mullen, K.; Osuma, A.; Lo Schiavo, G. Y.; Wilson, N. S. Preparation of indazolones as modulators of TNF signaling. PCT Int. Appl. WO2016168633A1, 2016.
(22) Congreve, M.; Carr, R.; Murray, C.; Jhoti, H. A 'rule of three' for fragment-based lead discovery? *Drug Discovery Today* **2003**, *8*, 876−877.
(23) Schubert, D.; Maier, B.; Morawietz, L.; Krenn, V.; Kamradt, T. Immunization with glucose-6-phosphate isomerase induces T cell-dependent peripheral polyarthritis in genetically unaltered mice. *J. Immunol.* **2004**, *172*, 4503−4509.
(24) Espada, A.; Broughton, H.; Jones, S.; Chalmers, M. J.; Dodge, J. A. A binding site on IL-17A for inhibitory macrocycles revealed by hydrogen/deuterium exchange mass Spectrometry. *J. Med. Chem.* **2016**, *59*, 2255−2260.
(25) Liu, S.; Desharnais, J.; Sahasrabudhe, P. V.; Jin, P.; Li, W.; Oates, B. D.; Shanker, S.; Banker, M. E.; Chrunyk, B. A.; Song, X.; Feng, X.; Griffor, M.; Jimenez, J.; Chen, G.; Tumelty, D.; Bhat, A.; Bradshaw, C. W.; Woodnutt, G.; Lappe, R. W.; Thorarensen, A.; Qiu, X.; Withka, J. M.; Wood, L. D. Inhibiting complex IL-17A and IL-17RA interactions with a linear peptide. *Sci. Rep.* **2016**, *6*, No. 26071.
(26) Chen, J.; Song, Y.; Bojadzic, D.; Tamayo-Garcia, A.; Landin, A. M.; Blomberg, B. B.; Buchwald, P. Small-molecule inhibitors of the CD40-CD40L costimulatory protein-protein interaction. *J. Med. Chem.* **2017**, *60*, 8906−8922.
(27) Silvian, L. F.; Friedman, J. E.; Strauch, K.; Cachero, T. G.; Day, E. S.; Qian, F.; Cunningham, B.; Fung, A.; Sun, L.; Shipps, G. W.; Su, L.; Zheng, Z.; Kumaravel, G.; Whitty, A. Small molecule inhibition of the TNF family cytokine CD40 ligand through a subunit fracture mechanism. *ACS Chem. Biol.* **2011**, *6*, 636−647.
(28) Hong, S. S.; Choi, J. H.; Lee, S. Y.; Park, Y. H.; Park, K. Y.; Lee, J. Y.; Kim, J.; Gajulapati, V.; Goo, J. I.; Singh, S.; Lee, K.; Kim, Y. K.; Im, S. H.; Ahn, S. H.; Rose-John, S.; Heo, T. H.; Choi, Y. A novel small-molecule inhibitor targeting the IL-6 receptor beta subunit, Glycoprotein 130. *J. Immunol.* **2015**, *195*, 237−245.
(29) Todorović, V.; Su, Z.; Putman, C. B.; Kakavas, S. J.; Salte, K. M.; McDonald, H. A.; Wetter, J. B.; Paulsboe, S. E.; Sun, Q.; Gerstein, C. E.; Medina, L.; Sielaff, B.; Sadhukhan, R.; Stockmann, H.; Richardson, P. L.; Qiu, W.; Argiriadi, M. A.; Henry, R. F.; Herold, J. M.; Shotwell, J. B.; McGaraughty, S. P.; Honore, P.; Gopalakrishnan, S. M.; Sun, C. C.; Scott, V. E. Small molecule IL-36gamma antagonist as a novel therapeutic approach for plaque psoriasis. *Sci. Rep.* **2019**, *9*, 9089−10004.
(30) McCoy, A. J.; Grosse-Kunstleve, R. W.; Adams, P. D.; Winn, M. D.; Storoni, L. C.; Read, R. J. Phaser crystallographic software. *J. Appl. Crystallogr.* **2007**, *40*, 658−674.
(31) Vonrhein, C.; Flensburg, C.; Keller, P.; Sharff, A.; Smart, O.; Paciorek, W.; Womack, T.; Bricogne, G. Data processing and analysis with the autoPROC toolbox. *Acta Crystallogr., Sect. D: Biol. Crystallogr.* **2011**, *67*, 293−302.
(32) Bricogne, G.; Blanc, E.; Brandl, M.; Flensburg, C.; Keller, P.; Paciorek, W.; Roversi, P.; Smart, O.; Vonrhein, C.; Womack, T. *BUSTER-TNT v.2.11.7*; Global Phasing Ltd.: Cambridge, U.K., 2019.
(33) Emsley, P.; Lohkamp, B.; Scott, W. G.; Cowtan, K. Features and development of Coot. *Acta Crystallogr., Sect. D: Biol. Crystallogr.* **2010**, *66*, 486−501.

https://dx.doi.org/10.1021/acs.jmedchem.0c01280
J. Med. Chem. 2021, 64, 417−429